Crystalline anisotropy of shock-induced phenomena: Omni-directional multiscale shock technique

Shimamura, Kohei ; Misawa, Masaaki ; Ohmura, Satoshi ; Shimojo, Fuyuki ; Kalia, Rajiv K. ; Nakano, Aiichiro ; Vashishta, Priya

(Citation)
Applied Physics Letters,108(7):071901-071901

(Issue Date)
2016-02-15

(Resource Type)
journal article

(Version)
Version of Record

AIP | Applied Physics Letters

Crystalline anisotropy of shock-induced phenomena: Omni-directional multiscale shock technique

Kohei Shimamura, Masaaki Misawa, Satoshi Ohmura, Fuyuki Shimojo, Rajiv K. Kalia, Aiichiro Nakano, and Priya Vashishta

Citation: Applied Physics Letters **108**, 071901 (2016); doi: 10.1063/1.4942191
View online: http://dx.doi.org/10.1063/1.4942191
View Table of Contents: http://scitation.aip.org/content/aip/journal/apl/108/7?ver=pdfcov
Published by the AIP Publishing

Crystalline anisotropy of shock-induced phenomena: Omni-directional multiscale shock technique

Kohei Shimamura,[1,2] Masaaki Misawa,[1,3] Satoshi Ohmura,[4] Fuyuki Shimojo,[1] Rajiv K. Kalia,[3] Aiichiro Nakano,[3] and Priya Vashishta[3]
[1]*Department of Physics, Kumamoto University, Kumamoto 860-8555, Japan*
[2]*Graduate School of System Informatics, Kobe University, Kobe 657-8501, Japan*
[3]*Collaboratory for Advanced Computing and Simulations, Department of Physics & Astronomy, Department of Computer Science, Department of Chemical Engineering & Materials Science, Department of Biological Sciences, University of Southern California, Los Angeles, California 90089-0242, USA*
[4]*Research Center for Condensed Matter Physics, Hiroshima Institute of Technology, Hiroshima 731-5193, Japan*

(Received 16 December 2015; accepted 5 February 2016; published online 16 February 2016)

We propose an omni-directional multiscale shock technique (OD-MSST) to study the shock waves in an arbitrary direction of crystalline materials, atomistically based on the molecular dynamics simulation method. Using OD-MSST, we found transitions from elastic to shear-banding to plastic behaviors for a model covalent crystal. In addition to such a shock "phase diagram," a transition from inter-molecular to intra-molecular mechanochemical reaction pathways was found as a function of crystallographic orientation in an energetic van der Waals crystal. © *2016 AIP Publishing LLC*.
[http://dx.doi.org/10.1063/1.4942191]

Understanding the propagation of shock waves in solids is of fundamental importance in many fields of science and technology,[1] including high-velocity impact[2] and detonation of explosives.[3] Of particular importance is the anisotropy of shock response, e.g., to design shock-absorbing heterostructures[4] or to understand the effect of crystallographic orientations on the sensitivity of energetic crystals.[5] A shock-wave front can be regarded as an interface that separates two different (i.e., unshocked and shocked) phases of material. This is compounded by various dynamic phase transitions, including shock-induced elastic-to-plastic[6] and structural[7–9] transitions. Nonequilibrium molecular dynamics (NEMD) simulations have been used extensively to study these shock-induced transitions at the atomistic level, where Newton's equations of motion for interacting atoms are solved on computers.[10] In particular, NEMD simulations have been used to study anisotropic shock.[11]

Direct NEMD simulations for shock-wave propagation require large system sizes and computational costs. Reed *et al.*[12] proposed a multiscale method that combines molecular dynamics (MD) simulations with the Euler equations for compressible flow to effectively encompass large time and length scales. In their multiscale shock technique (MSST), only a small part of the entire system is explicitly treated while the MD computational cell follows an equation of motion that is subject to macroscopic conservation laws of the mass, momentum, and energy for the shock, thereby reducing the computational cost significantly. The MSST has been implemented not only with empirical interatomic potentials[13] but also with quantum mechanical methods.[14–17]

The MSST has been applied to the study of crystalline anisotropy in shock response.[18] In the conventional MSST, however, the shock direction should coincide with one of the three lattice vectors that span the computational cell. This precludes continuous scan of the shock direction, and accordingly the study of shock anisotropy has been limited to a small set of low-index crystallographic orientations. To enable systematic study of shock anisotropy, where the shock direction is varied continuously, we propose an extended formulation of MSST, called omni-directional multiscale shock technique (OD-MSST).

Using OD-MSST, we found elastic-to-shear banding-to-plastic transitions in a model covalent crystal as the shock direction changes from [110] to [100]. In addition to these dynamic phase transitions, OD-MSST can probe orientation-dependent transitions of chemical reaction pathways. Specifically, we here report a transition from inter-molecular to intra-molecular mechanochemical reaction pathways as a function of the crystallographic orientation in an energetic van der Waals (vdW) crystal under high pressures and temperatures.

In MSST, the Lagrangian is defined as

$$L = \frac{1}{2}\sum_i m_i(\boldsymbol{h}\dot{\boldsymbol{q}}_i)^{\mathrm{t}}(\boldsymbol{h}\dot{\boldsymbol{q}}_i) - \Phi(\{\boldsymbol{h}\boldsymbol{q}_i\}, \boldsymbol{h}) + \frac{Q}{2M}\dot{V}^2 + \frac{1}{2}MV_{\mathrm{S}}^2\left(1 - \frac{V}{V_0}\right)^2 - P_0(V - V_0), \quad (1)$$

where m_i is the mass of the i-th atom, $\boldsymbol{q}_i$ is a vector whose components are the i-th atom's scaled coordinates in the range [0, 1], Φ is the potential energy, Q is a parameter with the unit of $(\text{mass})^2\cdot(\text{length})^{-4}$, $M = \sum_i m_i$ is the total mass of the system, and V_{S} is the speed of the shock wave. The real coordinates and velocities of the i-th atom are given by $\boldsymbol{h}\boldsymbol{q}_i$ and $\boldsymbol{h}\dot{\boldsymbol{q}}_i$, respectively, where $\boldsymbol{h} = (\boldsymbol{L}_1\boldsymbol{L}_2\boldsymbol{L}_3)$ is a matrix composed of the lattice vectors $\{\boldsymbol{L}_k\}$ of the computational cell. $V = \det\boldsymbol{h}$ is the volume of the computational cell. P_0 and $V_0 = \det\boldsymbol{h}_0$ are the pressure and volume of the unshocked state, respectively, where $\boldsymbol{h}_0$ corresponds to $\boldsymbol{h}$ in the unshocked state.

Since the shock is assumed to be planar, a uniaxial strain is allowed in the shock direction, and $\boldsymbol{h}$ has only one degree

of freedom. Usually, a rectangular parallelepiped computational cell is used, and the shock direction is selected to be parallel to one of the computational-cell lattice vectors.[12,14] In this paper, we show that these are not necessary conditions. Namely, the computational cell need not be a rectangular parallelepiped, and it is not necessary for the shock wave to be parallel to the cell vectors. This relaxation of conditions allows us to investigate the effects of shock direction systematically, by continuously varying the shock direction for a single system.

Omni-directional multiscale shock technique: We assume that the direction of the shock wave is parallel to an arbitrary vector $\boldsymbol{l}_1$, and two vectors $\boldsymbol{l}_2$ and $\boldsymbol{l}_3$ are perpendicular to $\boldsymbol{l}_1$. If $\{\boldsymbol{l}_k\}$ are given by $\boldsymbol{l}_k = \boldsymbol{h}\boldsymbol{n}_k$, where $\boldsymbol{n}_k$ is a vector whose components are integers, a virtual computational cell with the cell vectors $\{\boldsymbol{l}_k\}$ can be defined for the present system. Two matrices defined as $\boldsymbol{l} = (\boldsymbol{l}_1\boldsymbol{l}_2\boldsymbol{l}_3)$ and $\boldsymbol{n} = (\boldsymbol{n}_1\boldsymbol{n}_2\boldsymbol{n}_3)$ are related via

$$\boldsymbol{l} = \boldsymbol{h}\boldsymbol{n} \text{ or } \boldsymbol{h} = \boldsymbol{l}\boldsymbol{n}^{-1}. \tag{2}$$

To apply a uniaxial strain along $\boldsymbol{l}_1$, only the magnitude of $\boldsymbol{l}_1$ is allowed to change, and $\boldsymbol{l}_2$ and $\boldsymbol{l}_3$ transverse to the shock direction are kept fixed. In order to achieve these conditions, a dynamical variable γ is introduced as

$$\boldsymbol{l}_1 = \gamma\boldsymbol{l}_1^0, \quad \boldsymbol{l}_2 = \boldsymbol{l}_2^0, \quad \boldsymbol{l}_3 = \boldsymbol{l}_3^0, \tag{3}$$

where $\boldsymbol{l}_k^0 = \boldsymbol{h}_0\boldsymbol{n}_k$. By inserting Eq. (3) into Eq. (2), we obtain $\boldsymbol{h}$ as a function of γ

$$\boldsymbol{h} = \boldsymbol{h}_0(\boldsymbol{\alpha}\gamma + \boldsymbol{\beta}), \tag{4}$$

where $\boldsymbol{\alpha}$ and $\boldsymbol{\beta}$ are constant matrices determined by $\boldsymbol{n}$, i.e., the shock wave direction. Specifically, $\boldsymbol{\alpha}_{ij} = \boldsymbol{n}_{i1}\boldsymbol{n}_{1j}^{-1}$, $\boldsymbol{\beta}_{ij} = \boldsymbol{n}_{i2}\boldsymbol{n}_{2j}^{-1} + \boldsymbol{n}_{i3}\boldsymbol{n}_{3j}^{-1}$.

The equations of motion for $\boldsymbol{q}_i$ and γ are given by

$$\ddot{\boldsymbol{q}}_i = \boldsymbol{h}^{-1}\left[\frac{\boldsymbol{F}_i}{m_i} - \left\{(\dot{\boldsymbol{h}}\boldsymbol{h}^{-1})^{\mathrm{t}} + \dot{\boldsymbol{h}}\boldsymbol{h}^{-1}\right\}\boldsymbol{h}\dot{\boldsymbol{q}}_i\right], \tag{5}$$

$$\ddot{\gamma} = \frac{M}{Qf^2}\mathrm{tr}\left[\left\{\boldsymbol{\pi} - P_0\boldsymbol{I} - V_{\mathrm{S}}^2\frac{M}{V_0}\left(1 - \frac{V}{V_0}\right)\boldsymbol{I}\right\}\boldsymbol{X}\right], \tag{6}$$

respectively, where $\boldsymbol{X} = \boldsymbol{h}_0\boldsymbol{\alpha}V\boldsymbol{h}^{-1}$ and $f = \mathrm{tr}(\boldsymbol{X})$. $\boldsymbol{F}_i$ is the force acting on the i-th atom, $\boldsymbol{\pi}$ is the internal stress tensor, and $\boldsymbol{I}$ is the unit matrix. Note that $\boldsymbol{X}$ does not depend on γ. The proposed OD-MSST is a generalization of MSST for an arbitrary shock direction. Specifically, the equation of motion, Eq. (6), along with the parameterization of the shock direction, Eq. (4), constitute the generalization. When the shock direction coincides with one of the computational-cell vectors, the OD-MSST equation of motion becomes identical to that of MSST. In such cases, the energy and stress of MD simulations according to Eqs. (5) and (6) have been shown to obey the Hugoniot relations for a shock wave moving at a speed V_{S} within a reasonable accuracy.[19] When the shock direction is not aligned with a computational-cell vector, we have verified the accuracy of OD-MSST as shown in Fig. S1 in the supplementary material.[20]

Anisotropic shock phase diagram in a covalent crystal: To demonstrate the use of OD-MSST, we first simulate shock waves propagating in a model solid described by the Stillinger-Weber potential parameterized for silicon.[21] This system was used to test the original MSST,[12] and is important for various applications, including energetic materials.[22] We use a 512-atom system in an initial cubic supercell with a side length of 21.75 Å, which gives a zero-pressure diamond structure with its [100], [010], and [001] directions along the supercell sides. The equations of motion are solved using an explicit reversible integrator[23] with a time step of 1.2 fs. Simulations are performed for the time duration of 12 ps. First, we consider a shock wave propagating in the [110] direction. For the cubic supercell, this is achieved by using the following matrices:

$$\boldsymbol{\alpha} = \begin{pmatrix} 1/2 & 1/2 & 0 \\ 1/2 & 1/2 & 0 \\ 0 & 0 & 0 \end{pmatrix}, \quad \boldsymbol{\beta} = \begin{pmatrix} 1/2 & -1/2 & 0 \\ -1/2 & 1/2 & 0 \\ 0 & 0 & 1 \end{pmatrix}. \tag{7}$$

Figure 1 shows the calculated particle (or piston) velocity V_{P} as a function of the speed V_{S} of a shock wave propagating in the [110] direction. There is a discontinuous change in V_{P} at $V_{\mathrm{S}} = V_{\mathrm{S}}^* = 9.84$ km/s, which corresponds to an elastic-to-plastic transition. The relationship between the longitudinal pressure and the volume of shock states is shown in the inset, where the labels A and B correspond to those in the main plot.

For shock speeds slower or faster than V_{S}^*, a single elastic or plastic wave propagates, as shown in Fig. 2(a). In the double-shock regime between the states labeled A and B in Fig. 1, on the contrary, a second wave follows the first elastic wave. By using state A as an unshocked state in MSST simulations, we obtain the second shock speed in the double-shock regime,[12] which is indicated by the open green squares in Fig. 2(a). The square symbols in Fig. 2(a) indicate plastic waves, which are accompanied by disordering of atomic positions as indicated by the right inset of Fig. 2(a).

Next, we investigate a shock wave propagating in the [100] direction. Figure 2(b) shows that a single elastic wave exists below a particle velocity of $V_{\mathrm{P}} \sim 1.75$ km/s. Above this V_{P}, a second wave follows the faster elastic wave. In contrast to the [110] direction, we have found that the second wave is not accompanied by plastic deformation, but rather propagates with shear deformation on the (111) plane, as

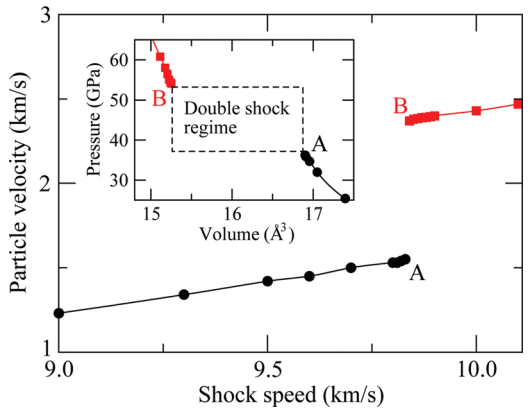

FIG. 1. Particle velocity as a function of the speed of a shock wave propagating in the [110] direction of a model diamond crystal. The inset shows the pressure-volume shock Hugoniot.

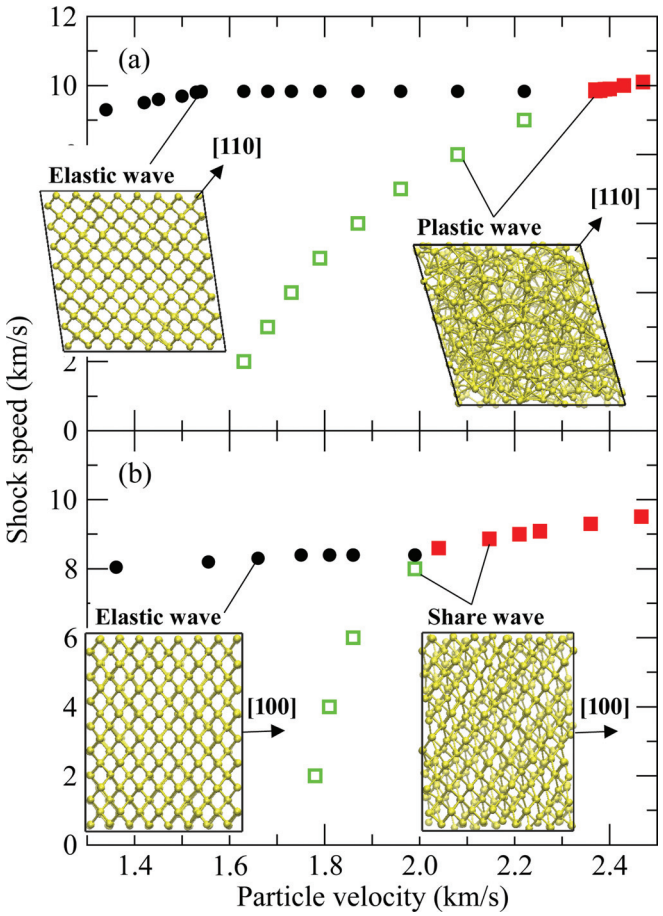

FIG. 2. Hugoniot relationships between shock speed and particle velocity for (a) [110] and (b) [100] directions. The circles indicate the shock speed of an elastic wave. The squares in (a) and (b) denote plastic and shear waves for the [110] and [100] directions, respectively. The snapshots in the inset show different shock responses.

shown in the right inset of Fig. 2(b). The coordination number of atoms in this shear wave is 4, the same as in the elastic wave, while that in the plastic wave in the [110] direction is $5 \sim 6$. It is known that shock-induced bond breaking rarely occurs in the [100] direction of the diamond structure because internal strain (which favors static displacement of atoms in the lateral directions) is not induced in [100] compression.[24] Our simulation reproduces this difference in shock response. Similar shear-banding responses have been observed in MD simulations of shock in silicon[25] and germanium[26].

To systematically study shock waves between [110] and [100] directions, OD-MSST simulations are carried out for [210], [310], and [410] directions. Unlike the original MSST, which requires a distinct computational cell for each of these directions,[12,19] OD-MSST requires only one computational cell to be set up, where simply $\boldsymbol{\alpha}$ and $\boldsymbol{\beta}$ parameters are varied to study different directions, resulting in vast reduction of efforts. Figure 3 shows a "phase diagram" for shock waves. In regions I, II, and III, only a single elastic, shear, and plastic shock wave propagates, respectively. The striped areas correspond to double-shock regimes, in which a faster (elastic or shear) wave precedes a slower (shear or plastic) wave. It is seen that the boundary between regions I and II, i.e., between elastic and shear waves, depends weakly on the shock wave direction. On the other hand, the double-shock region between

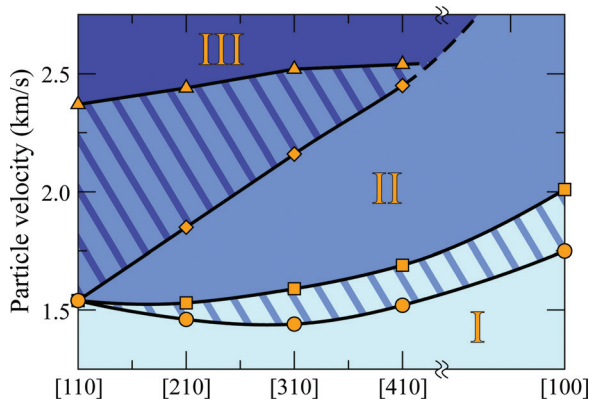

FIG. 3. "Phase diagram" for shock waves. In regions I, II, and III, only a single elastic, shear, and plastic shock wave propagates, respectively. In the striped areas, a faster (elastic or shear) wave precedes a slower (shear or plastic) wave.

regions II and III, i.e., between shear and plastic waves, becomes narrower near [100] direction, and finally, the plastic wave disappears for [100] direction.

Anisotropic mechanochemistry of a van der Waals crystal: Next, we apply OD-MSST to the triclinic molecular crystal of triaminotrinitrobenzene (TATB). TATB is a rather insensitive aromatic explosive, based on the basic six-carbon benzene ring structure with three nitro functional groups (NO_2) and three amine (NH_2) groups attached, alternating around the ring. In addition, it belongs to a broad class of layered molecular crystals that are bonded by inter-layer vdW interactions.[27,28] Within each layer, these crystals are inter-bonded by a strong hydrogen-bond network as well as intra-molecular covalent bonds. Interplay between the inter-layer vdW and intra-layer hydrogen bonds is expected to dictate anisotropic detonation behaviors of these energetic vdW crystals.

To study shock-initiated chemical reactions, we perform quantum molecular dynamics (QMD) simulations, in which interatomic forces are calculated quantum mechanically.[20] The simulated supercell contains 8 TATB molecules (in total of 192 atoms) and has the lattice parameters, $a([100]) = 9.013$ Å, $b([010]) = 18.417$ Å, $c([001]) = 13.624$ Å, $\alpha = 108.58°$, $\beta = 91.82°$, and $\gamma = 119.97°$ (Fig. 4(a)). The lattice parameters are determined such that the axial stresses (P_{xx}, P_{yy}, and P_{zz}) become zero when performing structural optimization. Periodic boundary conditions are applied in all directions. Five OD-MSST simulations are performed, in which shock waves propagate in the crystallographic [001], [012], [011], [021], and [010] directions, respectively, with a shock speed of 10 km/s. Initial temperature is set to 300 K. The equations of motion are integrated numerically with a time step of 0.242 fs. Simulations are performed for the time duration of 1.21 ps. Supplementary movies, S1.mov–S5.mov, show the atomic trajectories of the OD-MSST simulations in [001], [012], [011], [021], and [010] directions, respectively.[20]

Since multiple layers are bonded only by weak vdW interaction, inter-molecular bonds along the shock direction perpendicular to the *ab* plane are very weak. When a shock is applied along this direction, molecules from neighboring layers repeatedly collide in an elastic-collision manner as shown in Fig. S2.[20] For [001], [012], and [011] directions,

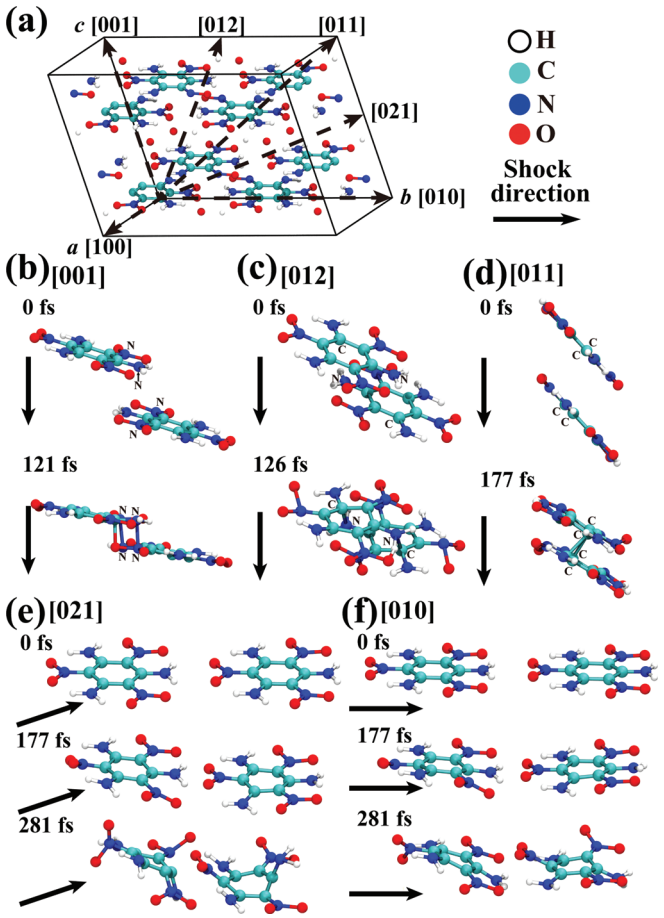

FIG. 4. (a) Initial atomic configuration in a $1 \times 2 \times 2$ supercell of triclinic TATB crystal. White, cyan, blue, and red spheres represent hydrogen, carbon, nitrogen, and oxygen atoms, respectively. (b)–(f) Anisotropic reaction dynamics shown by snapshots of part of the atomic configuration in [001] (b), [012] (c), [011] (d), [021] (e), and [010] (f) shocks. The angles from [010] direction are 108.58, 69.35, 42.53, 21.67, and 0 degrees for [001], [012], [011], [021], and [010] directions, respectively.

we observe that atoms from neighboring layers (that are positioned on top of each other along these directions) collide with each other repeatedly. Figures 4(b), 4(c), and 4(d) show snapshots of part of atomic configurations in [001], [012], and [011] direction shocks, respectively. Shortening of atomic distances between N–N, C–N, and C–C is observed at 121, 126, and 177 fs as shown in Figs. 4(b), 4(c), and 4(d), respectively. Although anti-bonding states are formed at these times, they become stable bonding states after several repeated collisions, accompanied by the breakage of originally bonded atoms. For example, the distances between C atoms in benzene rings and N atoms in amine groups become shorter in [012] shock. After N atoms make contacts with C atoms at 126 fs as shown in Fig. 4(c), H atoms associated with them are released. Electrons from the N atoms, which form bonds with the H atoms, are subsequently involved in the formation of bonds with C atoms. Meanwhile, each C atom in the benzene rings can form one more bond because the coordination number is 3 at 0 ps. Consequently, C-N bonds are easily formed in [012] shock. Similar mechanisms apply for bond formation in [001] and [011] shocks. Thus, shock-induced chemical reactions are initiated at these inter-molecular contacts, and the type of

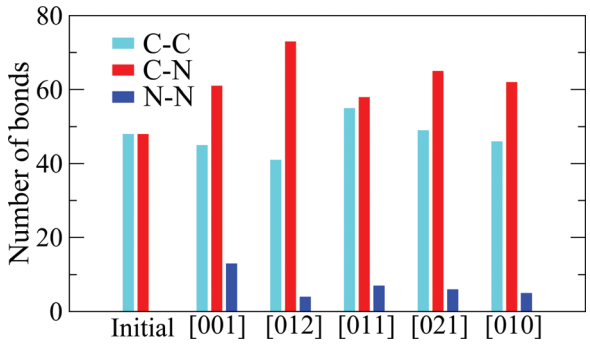

FIG. 5. The numbers of C–C, C–N, and N–N bonds at 1.21 ps in [001], [012], [011], [021], and [010] shock directions.

easily formed bonds is strongly affected by the shock direction for [001], [012], and [011] directions.

Shocks in [021] and [010] directions exhibit different deformation behaviors from those in the above three directions. Figures 4(e) and 4(f) show snapshots of part of the atomic configurations in [021] and [010] shocks, respectively. The angles of [021] and [010] directions from [010] are 21.64 and 0.00 degrees, respectively, which is much smaller than those in the above three directions. Accordingly, shock strength for the direction perpendicular to the *ab* plane is very weak, and thus deformation is dictated by the strong hydrogen-bond network in the *ab* plane. In these two directions, intra-layer collisions occur at 177 fs as shown in Figs. 4(e) and 4(f). The crystal structures, however, are not broken immediately. Instead, each molecule decomposes at 281 fs due to high accumulated strain arising from shock compression. In these directions, bond formation is governed by electronegativity (see later).

As shown in Fig. 5 and Fig. S3,[20] in [021] and [010] shocks, almost the same types of heteroatomic bonds (i.e., C–N and C–O) are mainly formed, which is understandable according to the electronegativity. In addition, an appreciable increase is observed only in the number of N–N bonds among homoatomic bonds in [021] and [010] shocks. This is because two N atoms from nitro- and amino-groups form a bond, since an O atom in the nitro-group extracts H atoms in the amino-group. On the other hand, in [001], [012], and [011] shocks, massive numbers of N-N, C-N, and C-C bonds are formed (Fig. 5). As mentioned earlier, this reflects geometrical arrangements of atomic positions during repeated inter-layer collisions. The profiles of the numbers of the bonds for the three directions differ considerably from those in [021] and [010] directions.

In summary, we have proposed OD-MSST to study shock waves in arbitrary crystallographic orientations, and demonstrated its applicability to systematic study of the orientational dependence of shock-induced phenomena. We found orientation-dependent elastic-to-shear banding-to-plastic transitions for a model covalent crystal and an inter-layer to intra-layer mechanochemical transition in an energetic vdW crystal.

We acknowledge the Supercomputer Center, Institute for Solid State Physics, University of Tokyo and the Research Institute for Information Technology, Kyushu University for the use of their facilities. The work at USC is partly supported by DTRA, Grant No. HDTRA1-14-1-0074.

[1]L. Davison, *Fundamentals of Shock Wave Propagation in Solids* (Springer-Verlag, Berlin, 2008).
[2]K. Tomeoka, K. Kiriyama, K. Nakamura, Y. Yamahana, and T. Sekine, Nature **423**(6935), 60–62 (2003).
[3]N. R. Greiner, D. S. Phillips, J. D. Johnson, and F. Volk, Nature **333**(6172), 440–442 (1988).
[4]S. M. Zhuang, G. Ravichandran, and D. E. W. Grady, J. Mech. Phys. Solids **51**(2), 245–265 (2003).
[5]J. M. Winey and Y. M. Gupta, J. Appl. Phys. **99**(2), 023510 (2006).
[6]B. L. Holian and P. S. Lomdahl, Science **280**(5372), 2085–2088 (1998).
[7]K. Kadau, T. C. Germann, P. S. Lomdahl, and B. L. Holian, Science **296**(5573), 1681–1684 (2002).
[8]P. S. Branicio, R. K. Kalia, A. Nakano, and P. Vashishta, Phys. Rev. Lett. **96**(6), 065502 (2006).
[9]Y. Z. Ma, M. Somayazulu, G. Y. Shen, H. K. Mao, J. F. Shu, and R. J. Hemley, Phys. Earth Planet. Inter. **143**, 455–467 (2004).
[10]B. L. Holian and G. K. Straub, Phys. Rev. Lett. **43**(21), 1598–1600 (1979).
[11]T. C. Germann, B. L. Holian, P. S. Lomdahl, and R. Ravelo, Phys. Rev. Lett. **84**(23), 5351–5354 (2000).
[12]E. J. Reed, L. E. Fried, and J. D. Joannopoulos, Phys. Rev. Lett. **90**(23), 235503 (2003).
[13]Y. Y. Ju, Q. M. Zhang, Z. Z. Gong, G. F. Ji, and L. Zhou, J. Appl. Phys. **114**(9), 093507 (2013).
[14]E. J. Reed, M. Riad Manaa, L. E. Fried, K. R. Glaesemann, and J. D. Joannopoulos, Nat. Phys. **4**(1), 72–76 (2008).
[15]C. J. Mundy, A. Curioni, N. Goldman, I. F. W. Kuo, E. J. Reed, L. E. Fried, and M. Ianuzzi, J. Chem. Phys. **128**(18), 184701 (2008).
[16]N. Goldman, E. J. Reed, I. F. W. Kuo, L. E. Fried, C. J. Mundy, and A. Curioni, J. Chem. Phys. **130**(12), 124517 (2009).
[17]L. A. Pellouchoud and E. J. Reed, J. Phys. Chem. A **117**(47), 12288–12298 (2013).
[18]T. R. Shan, R. R. Wixom, A. E. Mattsson, and A. P. Thompson, J. Phys. Chem. B **117**(3), 928–936 (2013).
[19]E. J. Reed, L. E. Fried, M. R. Manaa, and J. D. Joannopoulos, in *Chemistry at Extreme Conditions*, edited by M. R. Manaa (Elsevier, New York, 2005), pp. 297–326.
[20]See supplementary material at http://dx.doi.org/10.1063/1.4942191 for simulation methods and additional results.
[21]F. H. Stillinger and T. A. Weber, Phys. Rev. B **31**(8), 5262–5271 (1985).
[22]Y. Ohkura, J. M. Weisse, L. L. Cai, and X. L. Zheng, Nano Lett. **13**(11), 5528–5533 (2013).
[23]M. Tuckerman, B. J. Berne, and G. J. Martyna, J. Chem. Phys. **97**(3), 1990–2001 (1992).
[24]S. V. Zybin, M. L. Elert, and C. T. White, Phys. Rev. B **66**(22), 220102 (2002).
[25]G. Mogni, A. Higginbotham, K. Gaal-Nagy, N. Park, and J. S. Wark, Phys. Rev. B **89**(6), 064104 (2014).
[26]J. M. D. Lane and A. P. Thompson, AIP Conf. Proc. **1195**, 1157–1160 (2009).
[27]A. K. Geim and I. V. Grigorieva, Nature **499**(7459), 419–425 (2013).
[28]Z. F. Wang, Q. X. Li, H. B. Su, X. P. Wang, Q. W. Shi, J. Chen, J. L. Yang, and J. G. Hou, Phys. Rev. B **75**(8), 085424 (2007).